



**HAL**  
open science

## Local kinetics of cavitation in hydrogen-exposed EPDM using in-situ X-Ray tomography: focus on free surface effect and cavity interaction

Mahak Fazal, Sylvie Castagnet, Azdine Nait-Ali, Shin Nishimura

### ► To cite this version:

Mahak Fazal, Sylvie Castagnet, Azdine Nait-Ali, Shin Nishimura. Local kinetics of cavitation in hydrogen-exposed EPDM using in-situ X-Ray tomography: focus on free surface effect and cavity interaction. *Polymer Testing*, 2020, 10.1016/j.polymertesting.2020.106723 . hal-03022880

**HAL Id: hal-03022880**

**<https://hal.science/hal-03022880>**

Submitted on 25 Nov 2020

**HAL** is a multi-disciplinary open access archive for the deposit and dissemination of scientific research documents, whether they are published or not. The documents may come from teaching and research institutions in France or abroad, or from public or private research centers.

L'archive ouverte pluridisciplinaire **HAL**, est destinée au dépôt et à la diffusion de documents scientifiques de niveau recherche, publiés ou non, émanant des établissements d'enseignement et de recherche français ou étrangers, des laboratoires publics ou privés.

# Local kinetics of cavitation in hydrogen-exposed EPDM using in-situ X-Ray tomography: focus on free surface effect and cavity interaction

Mahak Fazal <sup>1</sup>, Sylvie Castagnet <sup>1\*</sup>, Azdine Nait-Ali <sup>1</sup>, Shin Nishimura <sup>2,3</sup>

<sup>1</sup> Institut Pprime (UPR 3346 CNRS – ENSMA – Université de Poitiers), Department of Physics and Mechanics of Materials, 1 Avenue Clément Ader, BP 40109, 86961 Futuroscope cedex, France

<sup>2</sup> Research Center for Hydrogen Industrial Use and Storage (HYDROGENIUS), Kyushu University, 744 Motooka, Nishi-ku, Fukuoka 819-0395, Japan

<sup>3</sup> Department of Mechanical Engineering, Kyushu University Graduate School of Engineering, 744 Motooka, Nishi-ku, Fukuoka 819-0395, Japan

## Abstract

Decompression failure in high-pressure gas exposed rubbers has almost only been studied at a global scale so far. In the present study in hydrogen-exposed EPDM, the growth kinetics of cavities was visualized and quantified for the first time at the cavity scale using 3D in-situ X-ray micro-tomography with an emphasis on interaction effects and boundary conditions. The volume evolution of cavities was processed and the inflation rate and maximum volume were calculated. The boundary conditions of selected cavities was analysed in terms of distance to the free surface as well as distance to other cavities. Proximity to the free surface was found to be a driving force for evolution of cavities up to a certain value beyond which the growth kinetics are more driven by other factors such as time of nucleation. No clear interaction effect was pointed out between cavities with the current spatial resolution.

**Keywords:** decompression failure; blistering; clusters; secondary cavities; edge effect

## 1. Introduction

Exposure of rubber materials to diffusive gases at high pressure and subsequent decompression leads to cavitation and cracking [1]. In the past, this phenomenon has been studied for different gas polymer systems, mainly in rubber and to a lesser extent in thermoplastics [2-15]. Recently, the renewed interest in hydrogen as an alternative energy carrier in the last decade has made studies around it more pertinent, decompression failure included. The application of rubber materials in the Fuel Cell Vehicles (FCVs) and the equipment used in the storage and transportation of hydrogen makes it important to study the compatibility of these materials with hydrogen specifically at high pressures, since hydrogen is kept at high pressures of up to 70MPa to improve its volume energy efficiency as a fuel [16-17].

The experimental studies on decompression failure in elastomers are few and often focused on qualitative analysis after the decompression had already taken place. This is due to the complex experimental techniques that are required to access the phenomenon in-situ. Besides, the properties of hydrogen and the safety measures associated with it lead to even more limitations in conducting experiments at the high pressure. Over the last decade, X-ray computed

---

\* corresponding author: sylvie.castagnet@ensma.fr

tomography technique has become very prominent in tracking defects and providing information on the microstructure of materials. In case of cavitation, this is especially useful, as in addition to the quantitative data measurements, it allows visualization of the damage, providing much needed data about the spatial distribution of the cavities in the material.

Focusing on hydrogen rubber systems, several studies have been conducted to track the damage in these systems [18-24]. The approaches of understanding the cavitation phenomenon could be either at the cavity field scale with several experimental works as well as numerical modelling in literature, or at the cavity scale, which has singularly been done via numerical modelling so far. Regarding experimental works at the scale of cavity fields, the work of Jaravel et al [21] should be noted for studying the decompression failure in silicone rubber to analyse the effects of different factors like saturation pressure and decompression rate on the onset of damage. They found that both factors contributed to the onset of cavitation; while a faster decompression rate lead to a faster onset of cavities, a contrary trend was observed in case of saturation pressure where higher saturation pressure lead to slower onset of cavities. Due to the very small size of individual cavities, no statistical analysis of the cavity field could be extracted in this rubber. This was addressed in the work done by Kane Diallo et al. [25] who analysed the statistics of the evolution of cavities and the effects of decompression conditions on it, in Ethylene Propylene Diene Monomer (EPDM) flat samples. They applied a covariogram method to 2D views of cavity fields obtained by visible light transmission. The work provided quantitative statistical data of cavity fields and discussed the features of a Morphological Representative Volume Element (MRVE) which further guided the Finite Element modeling of cavitation.

In numerical approach towards cavitation, some studies in literature postulated existing defects in the material [26-27], modelling the growth of this defect as hyperplastic hollow sphere problem[28]. Improvements in this approach include taking onto account the shear stresses to predict the onset of cavitation [29-30], addressing the influence of rubber constitutive law [31-35]and taking into account the parameter of surface tension [33-34]. These studies were focused on predicting a critical mechanical load for the onset of cavitation and did not take into account the coupled diffuso-mechanical loading that elastomers undergo during the real conditions of gas exposure. In this framework, in a more recent study, Jaravel et al [36] also developed a model with a hollow sphere inside hyper-elastic incompressible material to simulate the cavity growth scenario. They solved the problem in a coupled framework taking into account the sorption parameters as well as the elastic modulus of rubber. Consequently, they took into account the internal pressure of cavity, hydrogen content inside the cavity as well of the rubber matrix. This approach addressed the cavitation phenomenon at the cavity scale. However, due to the lack of experimental data at this scale as well as many assumptions, the results could be tentative at best even when providing an important step in understanding the cavitation phenomenon. In addition, the problem was solved in a 1D framework (along a radius), i.e. a pure hydrostatic framework. The proximity of another cavity could not be simulated.

The studies so far discussed were done using visible light transmission, which had strong limitation in terms of sample transparency and thickness, due to the bias introduced due to 2D rendering of a 3D damage field and overlapping issues. These constraints also limited the experimental quantification of the local cavity kinetics which was essential as a complement to

the numerical modelling to provide a robust understanding of the phenomenon as well as insight into the local interaction of cavities which so far has not been addressed in literature. Recent developments of time resolved 3D techniques for in-situ tracking of decompression failure have allowed for better quantification of characteristics of cavitation. For example, in a recent study by Euchler et al, X-ray microtomography was used to address onset and growth of cavities in unfilled SBR subjected to tensile deformation [37]. Castagnet et al. used this technique to study the decompression failure mechanism optimising the results previously obtained by 2D methods. They were able to better characterise the size and shape of an MRVE for the cavity field using covariogram analysis which was calculated to be much lesser than was computed by the 2D imaging [38]. This 3D characterisation of the cavity field allows more accurate estimations of damage evolution particularly in terms of efficient quantification of distances between cavities as well as their shape which gives a better idea of spatial distribution of cavities in the sample, and a possible anisotropic nature of the cavity itself. This robust quantification is important mainly to address the gaps in literature in terms of investigating local kinetics of cavities which is an essential step in verifying the local interactions of cavities and enrich the discussion on the complex processes that drive the nucleation, growth of cavities due to gas decompression. The complexity of the phenomenon of cavitation is related but not limited to its morphology and its relationship to cracking. An insight into this has been provided by various studies addressing the evolution of cavitation in rubber subjected to cyclic gas exposure and subsequent depressurisation [24,38].

Recently, Ono et al [40] investigated the damage evolution in EPDM subjected to successive cycles of high pressure hydrogen and decompression using in situ optical tracking. They observed that all the cavities appearing during the pressure release of the first cycle did not necessarily appear in the subsequent cycles leading to an important conclusion that the damage due to cavitation was not a cumulative process necessitating the experimental studies to be done efficiently at a cavity scale.

This study uses the 3D in-situ micro-tomography ( $\mu$ CT) to better understand the local phenomenon of cavitation like growth kinetics with emphasis on boundary conditions and interaction effects using the image analysis tool. This investigation could very well be the first step in providing much needed quantitative data of cavitation at a local scale to answer the questions of the processes that govern this phenomenon which have been raised in the previous studies [25, 40] but not investigated so far. This paper first provides the main characteristics of the tomography experiment; more details can be found in the earlier publication [38], which has been dedicated to this technique itself. Thereafter, the inflation characteristics of isolated cavities are discussed (especially as a function of their distance to the free surface) before comparing them with the inflation characteristics of close cavities and discriminate a possible interaction effect. The correlation between global desorption and the life of cavities is finally addressed using numerical simulations.

## **2. Experimental details**

### *2.1. Samples*

Experiments were performed on unfilled, peroxide-linked EPDM provided by Hydrogenius laboratory at Kyushu University, Japan. Different geometries of the samples (illustrated in

Figure 1) were chosen to ensure a practically suitable saturation time and to capture the damage in as much a representative way as possible at the global scale. Samples with dimensions of  $5 \times 5 \times 4$  mm and  $20 \times 20 \times 2$  were cut from  $15 \times 15$  cm compression molded sheets of 4 mm and 2 mm thickness respectively. These samples are henceforth referred to in the paper as Type-1 and Type-3 samples respectively. All samples were taken from the centre of the sheets to eliminate any inhomogeneity at the edge due to manufacturing processes. Additionally, 8 and 6 mm cubic samples, referred to as Type-2 samples, were cut from cylindrical samples of 29 mm height and 13 mm diameter to provide a relatively more representative sample for a global damage field observation with isotropic boundary conditions. Samples of two crosslink densities were tested, the details of which are listed in the Table 1.

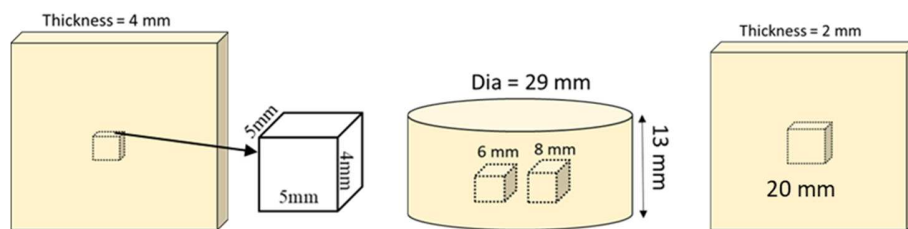


**Figure 1:** Schematic of samples: Type-1 ( $5 \times 5 \times 4$  samples from 4 mm thick flat sheets), Type-2 (cubic samples of 8 mm and 6 mm edge cut from 29 mm diameter cylinders) and Type-3 (rectangular samples of  $20 \times 20 \times 2$  mm cut from 2 mm thick flat sheets).

	EPDM 0.5	EPDM 1.6
crude rubber (ESPRENE 505) (phr)	100	100
Dicumyl Peroxide (crosslinking agent) (phr)	0.5	1.6
stearic acid (crosslinking accelerator) (phr)	0.5	0.5
crosslink density ( $\text{mol}/\text{cm}^3$ )	4.21E-05	2.81E-04
diffusion coefficient of hydrogen ( $\text{mm}^2/\text{sec}$ )	1.49E-04	1.89E-04

**Table 1:** Composition and properties of EPDM samples. The crosslink density was measured by swelling method and the diffusion coefficient was measured by thermal desorption analysis (TDA) [41]

## 2.2. Decompression conditions

Tests were carried out at two different decompression conditions:

(i) At a saturation pressure ( $P_{\text{sat}}$ ) of 8 MPa with a pressure release rate ( $\dot{P}$ ) of 1.6 MPa/min: samples of different cross-link densities were tested in the conditions to evaluate the effect of crosslinking of the size of cavities at a local scale. The tests were carried out in two separate experimental campaigns during which 18 samples were tested.

(ii) At saturation pressure of 12 MPa with a pressure release rate of 2.5 MPa/min: EPDM 1.6 samples of different geometries were tested in these conditions to evaluate the geometrical contribution to the kinetics and/or the morphology of cavities. These conditions were an extension of the tests carried out in previous studies on EPDM [25].

### 2.3. In-situ tomography set up

The in situ X-ray tomography was done using an Ultratom tomograph from RX Solutions®. The tomograph was fitted with the cylindrical pressure chamber [38], which was filled with hydrogen up to a pressure of 12 or 8 MPa and kept as such till saturation and subsequently decompressed remotely. The saturation time of each sample was calculated using Crank's equation for 1D diffusion through an infinite plate of thickness exposed to a constant gas content on each of the faces, while considering the diffusion to be Fickian [42, 43]. Consequently, the saturation times were overestimated as the diffusion from the lateral surfaces of the samples was not taken into account.

As already mentioned, more details of the  $\mu$ CT device and its working can be found elsewhere [38]. For the present study, the device was configured for the following acquisition parameters: Two hundreds projections taken over one hundred seconds corresponding to a complete 360° rotation. The acquisition was done for 3600 seconds starting at the beginning of decompression. The edge of the voxel measured was 16 $\mu$ m.

### 2.4. Data treatment

The images from the  $\mu$ CT were reconstructed using the XACT® software developed by RX solutions which is based on the filtered back projection algorithm. Various parameters like spot correction, ring artefact correction, contrast equalisation and offsetting of the image to account for the source displacement were carefully selected manually, adaptable to the raw images collected, to optimise the reconstruction for further post processing. The image processing was done using the Fiji plug-in of ImageJ® software as seen Figure 2 (a); various steps are illustrated in Figure 2. A dedicated macro for segmentation was defined for each sample after carefully calibrating the steps for optimum results. As seen in Figure 2 (b), prior to segmentation the images were cropped, to eliminate the noise and unusable data generated from an uneven surface. In the present study, the auto-thresholding filters of Huang, Intermodes or Isodata were used depending on the raw image. Various steps of noise removal were then applied; the resulting binarised image can be seen in Figure 2 (c). Figure 2 (d) shows the 3D visual of the complete cavitation field of the same binarised image. The 3D image was generated using the inbuilt 3D viewer function of Fiji.

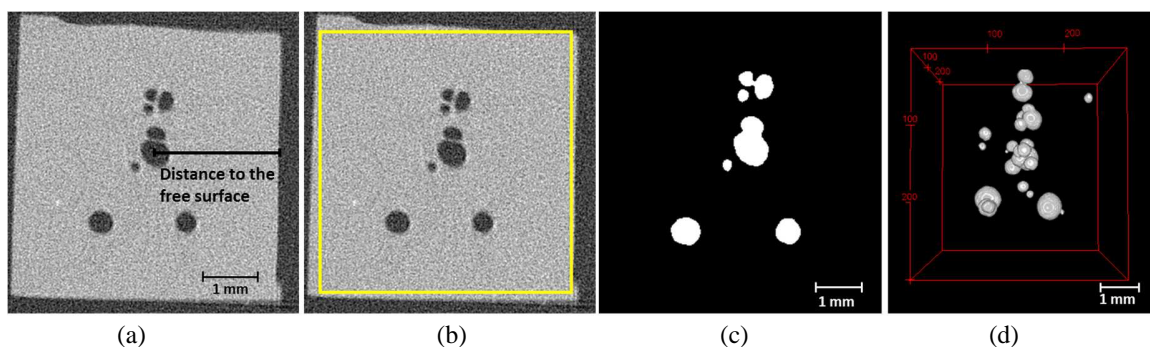


**Figure 2:** Steps of data processing illustrating (a) the reconstructed image used for calculation of distance to the free surface from the centre of the cavity (b) cropping the image to remove the uneven surface (c) binarisation (d) 3D view of the global cavitation field.

After image processing, a Matlab® code was used to generate 'vtk' format files for every sample as well as for labelling the cavities. The labelling ensured that the cavities could be tracked over time using the Paraview® software where any errors in the labelling process due to noise and other artefacts were eliminated.

Several parameters of the chosen cavities were calculated using 3D manager plugin of Fiji software: location, size, and distance between cavities when distinguishable with the current space resolution. The location refers to the centre of mass of the cavities. The volume of cavities was calculated at each time step by the method of counting voxels to minimise the over or underestimation introduced due to fitting with an ellipse. However, this method introduces certain artefacts when the size of the cavity is very small due to pixelisation.

Since the acquisition time for tomography was 100s for one reconstruction and therefore one volume estimation, the mid-point of the time step has been considered to plot the time evolution of morphological parameters.

As the image was cropped during the image processing to eliminate the noise generated from an uneven surface, the distance from the free surface was calculated taking the cropped voxels into account for each cavity manually. Hence, the distance from the free surface mentioned henceforth in the paper was the actual distance from the free surface of the sample and not of the cropped image, illustrated in Figure 2 (a).

### *2.5. Simulations of macroscopic gas desorption*

As a complement to the tomography, Finite Element (FE) simulations were carried out in Abaqus® to provide information on the diffusion characteristics of a homogenous unexposed sample at the macroscopic scale and to discuss some of the experimental trends. The simulation was done for a sample of 5x5x4 mm for a pure diffusion problem. The aim was to quantify the distribution of hydrogen content within the sample all along and after decompression, in order to discuss some of the observed phenomena.

The model consisted of the sample with the same dimensions as Type-1 sample, in a pure diffusion condition that was simulated as a heat transfer problem which is analogous to mass transfer if the value of density and specific heat is set as unity. The simulation was done for EPDM 1.6 which has a diffusion coefficient of 1.89E-4 mm<sup>2</sup>/sec. The model simulated the decompression stage of the hydrogen exposure, taking the initial state of the sample at equilibrium which was characterised by a predefined field of constant concentration of 8 MPa through the sample. The application of boundary conditions involved putting the concentration of the sample edges at zero mimicking the decompression phase of the hydrogen exposure for the conditions of  $P_{\text{sat}} = 8 \text{ MPa}$  and  $\dot{P} = 1.6 \text{ MPa/min}$ .

The sample was meshed with a standard linear heat transfer element of DC3D8 type. Prior to actual simulations, the test for mesh sensitivity was carried out for a regular mesh with different mesh sizes of 0.2, 0.1 and 0.05mm and the mesh size of 0.1 was taken to be most optimum for regular meshing.

## **3. Results and discussion**

### *3.1. A terminology for cavity populations based on morphology*

Cavities were locally selected from a global damage field and separated in three categories to evaluate the inflation characteristics and help a comprehensive analysis of interaction effects. For image processing, the cavities were fitted inside a box with side equal to the maximum diameter attained by the cavity all along the inflation / deflation process. In cases that the cavities could be contained in the box without any intrusion by other cavities, they were termed as “isolated cavities”, marked by yellow box titled ‘a’ in Figure 3 (a). The cavities that could not be contained in a single box without intrusion from other cavities during the whole evolution, but with a possible segmentation of them, were termed as “close cavities” marked by yellow box titled ‘b’ in figure 3 (a). Networks of very close cavities that were not visually distinguishable due to the limited resolution of the tomograph and could not be quantitatively analysed individually by the image processing software were called “clusters”, marked by yellow box titled ‘c’ in Figure 3 (a).

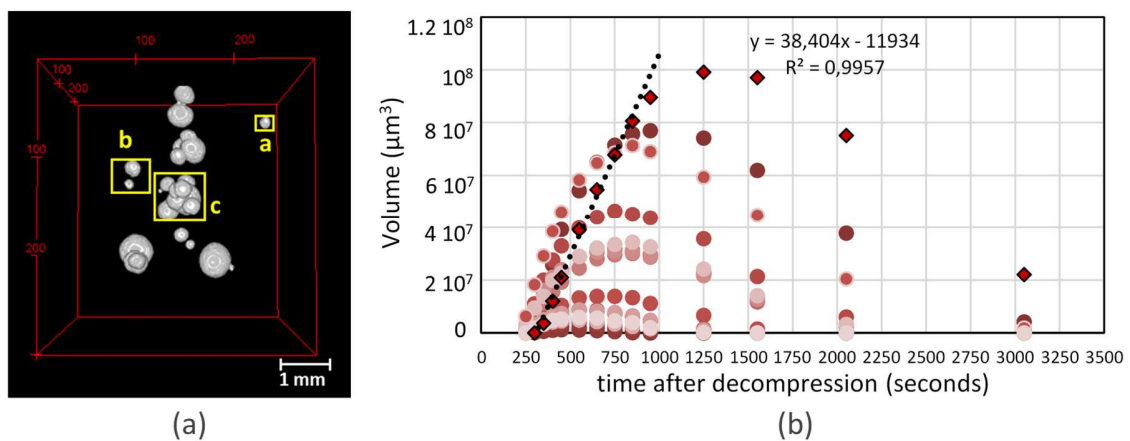


**Figure 3:** (a) Illustration of different cavity morphologies in Type-1 sample of EPDM 1.6 (b) volume expansion of selected isolated cavities of Type-1 sample of EPDM 0.5 saturated with hydrogen at 8 MPa and decompressed at 1.6 MPa/min. here, the curve with lined data points has been fitted to calculate the rate of inflation. This fitting was done for curves corresponding to all cavities to calculate their rate of inflation.

As mentioned above, the time evolution of size was measured for each of the selected cavities. It was plotted in voxels, keeping in mind that a voxel was  $16^3 = 4096 \mu\text{m}^3$ . The rate of inflation of each cavity was calculated by linearly fitting the first part of the curve. It is exemplified in Figure 3 (b) which shows the evolution of selected cavities of Type-1 sample of EPDM 0.5. In this figure, the curve with black lined data points has been linearly fitted in the expansion stage to exemplify the fitting process that was repeated for all the curves.

As already mentioned, artefacts introduced due to pixelisation are most prominent in smaller volumes, making the first detected volume of the cavity rather unreliable. This effect is further intensified due to fast kinetics in the earliest inflation stage, typical of cavities nucleated during the earliest stage of decompression i.e., within 200 seconds after decompression. Due to this, the first data point for first nucleating cavities was generally omitted during the linear fitting of the curve to calculate the rate of inflation. However, for the cavities nucleated later and detected at sufficiently high value so as not to be severely affected by image processing biases, the linear

fitting included the first data point of calculated volume. Smallest cavities with very few data points (less or equal to 3) in the range of inflation were excluded from this analysis.

### 3.2. Inflation characteristics of isolated cavities

Figure 4 shows the maximum volume ( $V_{\max}$ ) attained by the isolated cavities versus the distance from the free surface for the Type-1 samples of EPDM 1.6 and EPDM 0.5 exposed to the pressure conditions of  $P_{\text{sat}} = 8 \text{ MPa}$  and  $\dot{P} = 1.6 \text{ MPa/min}$ .

For both samples, the cavities showed an increasing trend in their maximum volume  $V_{\max}$  with the increase in their distance from the free surface. The cavities in EPDM 0.5 showed a rather linear trend in  $V_{\max}$  with very few outliers corresponding to the cavities that were close to two surfaces (star shaped markers), indicating an “edge effect”. The cavities closer to the free surface were characterised by lower  $V_{\max}$ , an effect which was intensified when the cavities were closer to two free surfaces.

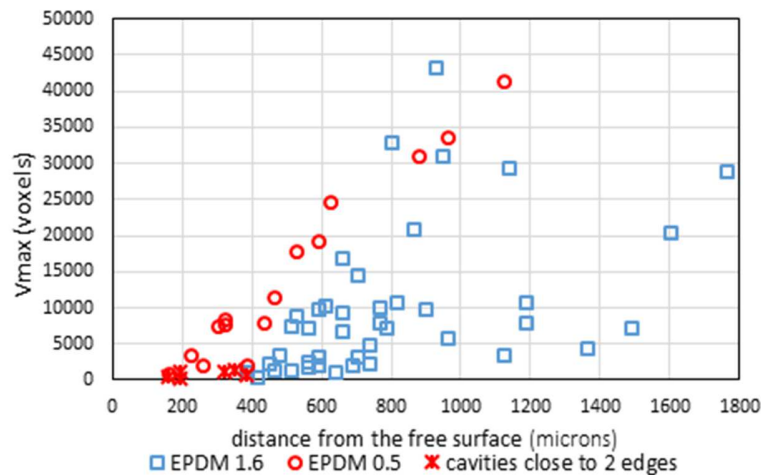


**Figure 4:** Effect of distance from the free surface on  $V_{\max}$  of isolated cavities (exposure conditions:  $P_{\text{sat}} = 8 \text{ MPa}$  and  $\dot{P} = 1.6 \text{ MPa/min}$ )

The same trend was observed in EPDM 1.6 too. Results were more scattered in EPDM 1.6, but since data points are fewer for EPDM 0.5 for cavities in the bulk, the difference could not be interpreted. Cavities in EPDM 0.5 showed a larger  $V_{\max}$  as compared to the more cross-linked EPDM 1.6. However, the direct relationship of cavity size and cross-link density would need to be done in a more statistical way.

The “bubble graph” in Figure 5 shows the rate of inflation of the same cavities as discussed above, as function of distance from the free surface. The size of the bubble corresponds to the maximum volume of the cavities. For scaling purpose, the size of a few of them (in voxel) was reminded in the graphs. The cavities for samples of EPDM 0.5 and 1.6 have been plotted in different graphs for the purpose of clarity. The rate of inflation showed a similar trend as the maximum volume  $V_{\max}$ . It sharply increased with the distance to the free surface for the cavities close to the edge, and turned more random and scattered (at least in EPDM 1.6), indicating that

the distance to the free surface was not a first order parameter for the cavities more towards the bulk of the samples. Except the comment on scatter which could be related again to the fewer data points in EPDM 0.5, these trends were similar in both samples, indicating that the change in crosslink density did not significantly affect the trends of the evolution of cavities at the local scale, within the explored range of crosslink densities. The cavities in which the “edge effect” was prominent have been termed as “edge cavities” whereas the cavities where this effect was not significant were termed as “bulk cavities” in the following. This classification allowed for a more comparative and step-by-step analysis of a process which in actuality occurs due to the convoluted effect of several parameters, as described in the subsequent sections.

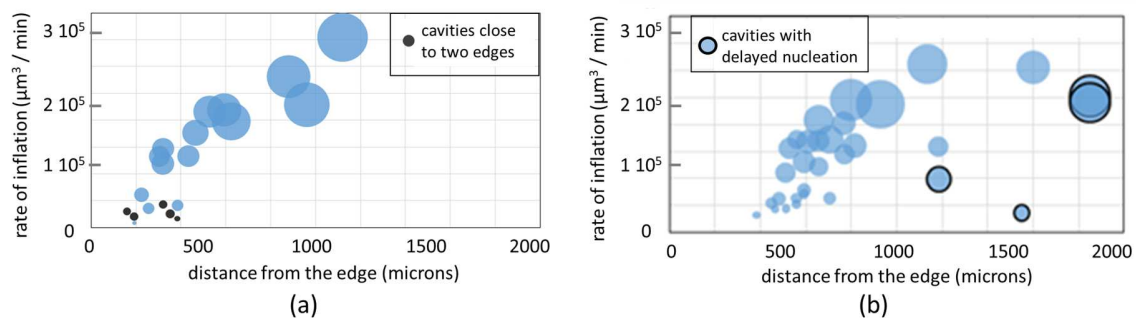


**Figure 5:** Effect of distance to the free surface on the rate of inflation and  $V_{\text{max}}$  of cavities from Type-1 sample of (a) EPDM 0.5. (b) EPDM 1.6 ( $P_{\text{sat}} = 8 \text{ MPa}$  and  $\dot{P} = 1.6 \text{ MPa/min}$ ). The circles with thick borders correspond to cavities with delayed nucleation. The maximum volume of the cavity is proportional to the bubble size.

In Figure 5 (b), the circles with thick borders corresponded to the cavities with delayed nucleation. In the literature, delayed nucleation has been termed as “secondary” cavities and referred to a cluster of satellite cavities surrounding the earlier nucleated ones (referred to as primary cavities) [44]. However, in the present study delayed cavities (termed as secondary cavities) did nucleate later than the initial ones (termed as primary) (i.e. 350 to 500 seconds after decompression instead of 150-300 seconds after decompression for primary ones) but were not seen to necessarily nucleate closer to the initial ones. Unlike the primary ones, all the observed secondary cavities were located in the bulk.

Secondary cavities showed slower kinetics than the primary cavities appearing in the same sample and exposed to the same decompression conditions, and were mostly detected when the mechanical pressure on the sample exerted by the gas in the chamber was completely released. Although it was difficult to pinpoint the time of nucleation of a cavity in absolute terms, due to space and time resolution of the tomography acquisition, a contributing factor that could be conceived for the slower kinetics could be the different iso-conditions due to global desorption, leading to different boundary conditions in terms of local gas concentration. This question was addressed with simulations of global desorption and is detailed in the subsequent sections of the article.

The nucleation of primary cavities was always random in all samples suggesting that the nucleation of cavities is a local process. The secondary cavities were exclusively bulk cavities since the gas content at the edge is quicker to desorb.

Figure 6 compares the rate of inflation of isolated cavities in EPDM 1.6 Type-1 samples in two different pressure conditions. The blue dots correspond to the former exposure conditions ( $P_{\text{sat}} = 8 \text{ MPa}$  and  $\dot{P} = 1.6 \text{ MPa/min}$ ) while the yellow ones correspond to more drastic decompression conditions:  $P_{\text{sat}} = 12 \text{ MPa}$  and  $\dot{P} = 2.5 \text{ MPa/min}$ .

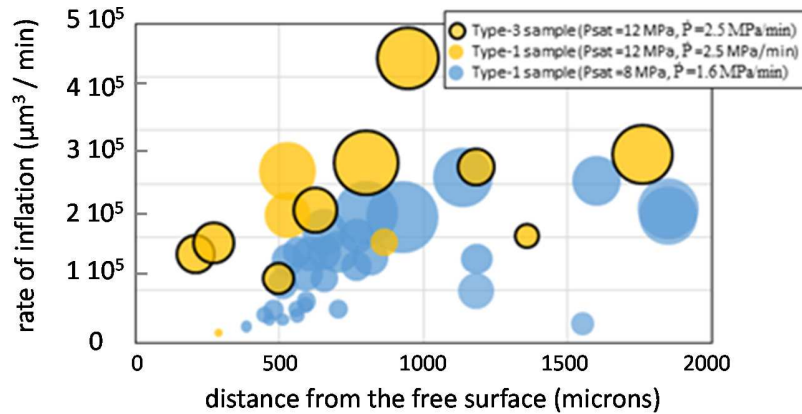


**Figure 6:** Effect of decompression conditions and sample geometry on the rate of inflation and maximum volume  $V_{\text{max}}$  (proportional to the dot size) of all isolated cavities in EPDM 1.6.

The cavities in samples subjected to more drastic decompression conditions had a faster growth rate than the cavities under less intense decompression conditions even as they occur at the same distance from the free surface, as suggested by the global vertical shift of data points in Figure 6. The blue spheres at 500 microns from the free surface as seen in the graph show a growth rate of 10-30 voxels per min whereas the yellow spheres show the growth rate of 25 to 70 voxels per min. It should be noted that the cavities corresponding to the more drastic decompression conditions were picked up from samples with different dimensions while cavities corresponding to the blue dots have all been taken from Type-1 samples. The yellow dots with thick boundaries corresponded to cavities in Type-3 samples whereas the un-circled ones corresponded to cavities taken from Type-1 samples. The rate of inflation or maximum volume showed no trend with respect to geometry as the data points overlapped in the graph, suggesting that within this range the shape of the sample did not affect the growth kinetics of the cavities at the local scale. The distance to the free surface remained the dominant limiting factor for the growth of edge cavities irrespective of the geometry of the sample.

### 3.3. Inflation characteristics of close cavities

The characteristics of close cavities were analysed taking isolated cavities as a reference, in order to discuss the possible interaction effects. As introduced earlier, the close cavities referred to cavities close enough that each of them could not be isolated within a box during their growth, but distant enough that they could be separated from each other during the segmentation process. Groups of close cavities were taken from the global damage field of Type-1 and Type-3 samples of EPDM 1.6.

The kinetics of close cavities are discussed in the following section by considering specific events of close cavities in the bulk or at the edge. Since it was not always possible to address the factors affecting the kinetics of cavitation (e.g. closeness to edge, time of nucleation, closeness to another cavity) in a rigid sequential way, these aspects have sometimes been addressed simultaneously in the following cases.

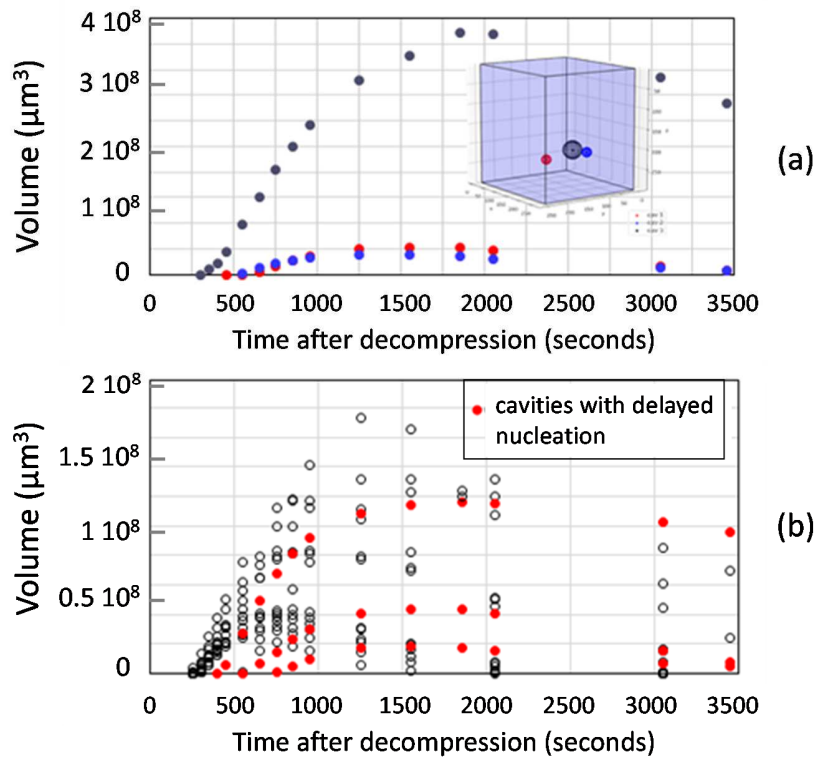


**Figure 7:** Volume evolution of (a) selected "bulk" cavities (b) all isolated bulk cavities taken from cavity field of Type-1 EPDM 1.6 sample saturated with hydrogen at 8 MPa and decompressed at 1.6 MPa/min

The first case is illustrated in Figure 7 (a) which shows the evolution of three cavities in bulk (1200-1500 microns from the free surface) in Type-1 sample of EPDM 1.6 exposed at the pressure conditions of  $P_{\text{sat}} = 8$  MPa and decompression rate of 1.6 MPa/min. The larger cavity was termed as the primary cavity as it nucleated first. One of the two secondary cavities (in blue) nucleated closer to the primary cavity (70 microns between borders) while the other secondary cavity (in red) nucleated farther from the primary cavity (250 microns between borders) but at the same time. The rate of inflation and maximal volume of these two secondary cavities were almost the same even after having different boundary conditions. The lower volume and rate of inflation was, therefore, attributed to the delayed nucleation rather than different local boundary conditions. Additionally, the evolution of the larger cavity remained unaffected by the nucleation of another cavity close to it. This could be supported by comparing the kinetics of these cavities to those of isolated bulk cavities as shown to Figure 7 (b). It was clear that the primary cavity show as black cavity in Figure 7 (a) showed similar volume evolution as that of isolated cavities shown in the graph in Figure 7 (b) as black unfilled circles.

On the other hand, the secondary cavities showed similar kinetics as those of isolated cavities with delayed nucleation shown in the graph of Figure 7 (b) as red filled circles. This could be further supported by looking at graphs in Figure 8 (a) and (b) that showed the volume evolution of groups of close cavities taken from Type-3 samples of EPDM 1.6 consisting of 2 and 3 cavities respectively.

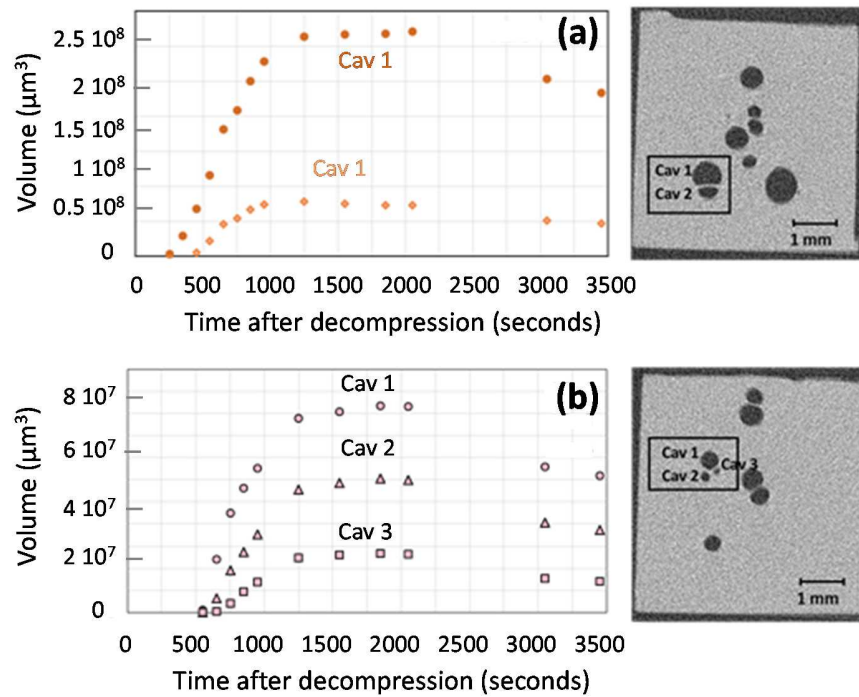


**Figure 8:** Volume evolution of groups of cavities taken from Type-3 samples of EPDM 1.6. The image to the right shows the respective cavities numbered in order of appearance.

In the graph in Figure 8 (a), secondary cavity showed a softer slope for inflation as well as deflation which is characteristic of cavities with a delayed nucleation. The same trend was seen second graph in Figure 8 (b) which shows the volume evolution of a group of close cavities consisting entirely of cavities with delayed nucleation (onset time about 500 s). The characteristic graph for delayed cavities was also seen here for all three cavities. Again, volume evolution of these close cavities could be compared to those of isolated cavities as seen in Figure 7 (b). It should also be noted that the primary cavity (the first detected cavity) was always the largest in size.

Similar content has been published in: Fazal M, Castagnet S, Nait-Ali A, Nishimura S. Local kinetics of cavitation in hydrogen-exposed EPDM using in-situ X-Ray tomography: focus on free surface effect and cavity interaction, *Polymer Testing*, 91, 106723, 2020, <https://doi.org/10.1016/j.polymertesting.2020.106723>

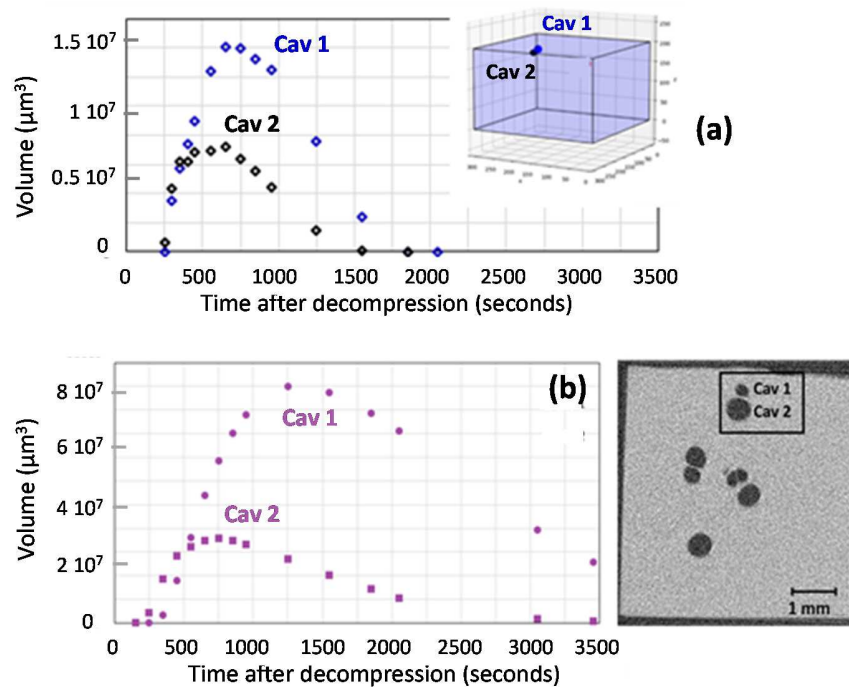


**Figure 9:** Volume evolution of groups of cavities taken from the cavity field of (a) Type-1 EPDM 1.6 sample. (b) Type-3 EPDM 1.6 sample. The image to the right in (b) shows the respective cavities which are numbered in order of appearance.

In the second case, we observed the kinetics of close cavities close to the edge of the sample. Figure 9 (a) shows the volume evolution of a pair of close cavities close to the free surface (600-800 microns), as illustrated in the schematic selected from the cavity field of Type-1 sample of EPDM 1.6 exposed to the same decompression conditions as discussed above for bulk cavities. These cavities showed very low maximum volume in comparison to some isolated cavities picked up from the same samples and plotted in Figure 7 (b). However, these close cavities show a shorter “lifetime” as compared to the bulk cavities. Since these close cavities were close to the edge as well, the shorter lifespan could either be attributed to the “edge effect” or to the proximity of another cavity. This could be made clear by looking at the volume evolution of close cavities taken from the cavity field of Type-3 EPDM 1.6 sample shown in Figure 9 (b). As can be seen from the graph, contrary to the normal trend, the primary cavity did not inflate to be the largest cavity. This could be explained by the edge effect since the primary cavity was closer to the free surface (516  $\mu\text{m}$ ); it behaved as an edge cavity resulting in lower volume in comparison with the secondary cavity. The secondary cavity showed the same trend of evolution as isolated cavities. It is safe to conclude that the proximity to the cavities did not lead to the same boundary conditions as the proximity to the free surface; indeed the latter remains to be the first order parameter affecting the kinetics of the growth of cavities. Nevertheless, limitations of the resolution should be highlighted here when considering the minimum distance between close cavities.

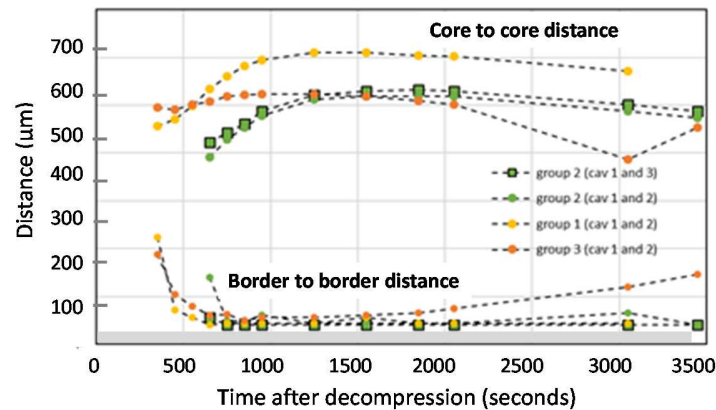


**Figure 10:** Distances between three groups of close cavities which are represented by yellow, green and orange markers respectively. The cavities of group 1 and group 2 have been shown in Figure 8. Group 3 has been shown in Figure 9 (b)

Figure 10 shows the evolution of distances between the centres of mass and borders of primary and secondary cavities of three groups of close cavities.

The distance between the centres of mass of the primary and the secondary cavities, which is denoted in the upper half of the graph, was never below 18-20 pixels while the minimum distance between the borders of the cavities, seen in the lower part of the graph was 2 pixels.

As seen in this Figure, the core to core distance of the cavities increased and then decreased. This initial increase could be as a result of increase in the bulk volume of the sample after the pressure release. In the later part, the decrease in the core to core distance was consistent with the global decrease in volume of the sample due to desorption. The border to border distance decreased sharply at first and then remained constant. It was highly probable that the decrease of the distance between the cavity borders during inflation was not quantifiable with the current resolution. However, the increase in the border to border distance was visible during the deflation stage as seen in the graph. The minimum distance between the cavity walls of two very close cavities could be found much less than this value with higher resolution experiments carried out in synchrotron facilities. Looking at the core to core distance, we are able to postulate the upper limit for the distance between cavities to form a group and thus be distinguished from the so called isolated cavities as 290 to 320  $\mu\text{m}$ . Again, a minimum distance between the cores of the cavities could not be assigned owing to the limitation of the image processing software in discretizing the very close cavities; indeed, it was possible that some cavities nucleate closer to each other than the ones investigated here.

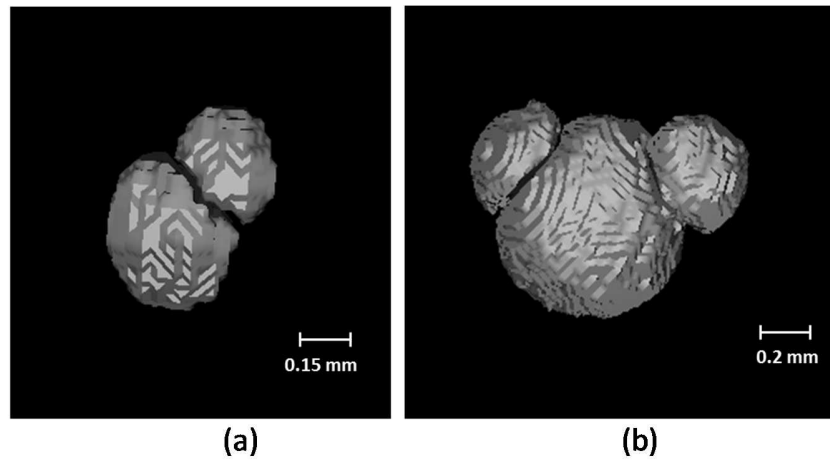


**Figure 11:** Selected groups of close cavities from Type-1 sample of EPDM 1.6 saturated at 8 MPa and decompressed at 1.6 MPa/min consisting of (a) two and (b) three close cavities.

The major effect manifested due to closeness of cavities was that of anisotropy. In close cavities, the anisotropy was topological. When the close cavities became larger and very close to each other, they were seen to crowd the shape of the closest cavity as illustrated in Figure 11, which shows a group of cavities taken from Type-1 sample of EPDM 1.6. Figure 11 (a) shows the 3D view of the group of close cavities seen in Figure 9 (a) discussed in the earlier section. Cavities retained their spherical morphology in the areas where they were not crowded by the proximity of another cavity while becoming flat where the boundaries of the cavities were very close. This topological effect was more pronounced when the cavity was sandwiched between two cavities as is seen in Figure 11 (b) which shows another group of cavities taken from the same sample. This topological anisotropy was more pronounced in the smaller cavity, which in most cases was the secondary cavity, while the primary cavity being the larger one retained its shape to a larger degree.

### 3.4. Role of the macroscopic desorption on the “edge effect” and delayed nucleation

From the calculation of the hydrogen content distribution in the sample all along decompression and after it, this section aimed to highlight some of the above results about free surface effect on the growth kinetics and maximum volume of isolated cavities. Indeed, this global desorption analysis did not account for some local gas content field re-organisations which could arise from interacting close cavities.

Figure 12 (a) shows the map of the gas concentration field in Type-1 sample of EPDM 1.6 which was computed using FE simulations. The curves in Figure 12 (b) show the temporal evolution of hydrogen gas partial pressure (MPa) which was directly linked to the gas concentration through Henry’s law [45], along the path plotted in white in Figure 12 (a). The dotted line in Figure 12 (b) corresponds to the evolution of hydrogen concentration at the free surface of the sample, i.e. the applied pressure ramp during decompression. Thereafter, the series of curves shows the evolution of hydrogen concentration at different depth points along the path at the interval of 100 microns up to the centre of the specimen plotted as a solid red line.

Similar content has been published in: Fazal M, Castagnet S, Nait-Ali A, Nishimura S. Local kinetics of cavitation in hydrogen-exposed EPDM using in-situ X-Ray tomography: focus on free surface effect and cavity interaction, *Polymer Testing*, 91, 106723, 2020, <https://doi.org/10.1016/j.polymertesting.2020.106723>

As can be seen, a gradient appeared on the external surface of the sample at the beginning of the decompression which traveled through the bulk of the sample rapidly at first and then gradually, as the gas desorbed. The concentration decreased very sharply at the edge of the sample whereas the centre of it remained saturated longer time with a less sharp concentration decrease.

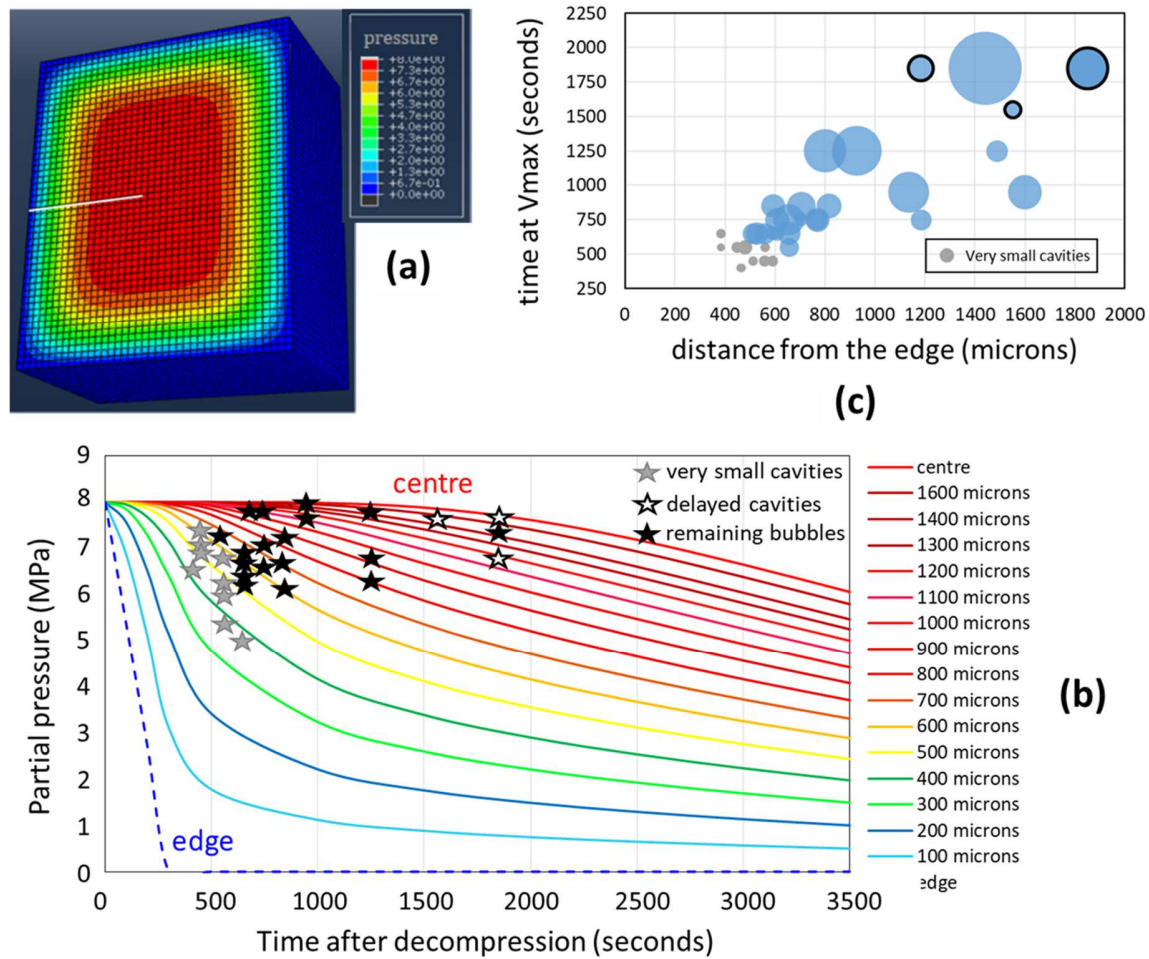


**Figure 12:** Correlation of macroscopic desorption with the kinetics of isolated cavities (a) Hydrogen concentration of Type-1 geometry at 1000 secs after decompression. The white line shows the path for which the curves of concentration gradient are plotted in (b). (c) Plots of time at  $V_{max}$  of isolated cavities taken from Type-1 sample of EPDM 1.6. The bubbles with thick borders correspond to the cavities with delayed nucleation. All these images were obtained from FE simulations.

The curves of global desorption shown in Figure 12 (b) were considered simultaneously with the graph shown in Figure 12 (c) which plots the time at which the isolated cavities have attained the maximum volume along their distance to the free surface. The size of the bubbles is representative of the relative maximum size of the cavities which are illustrated with stars in

the Figure 12 (b). In Figure 12 (b), three sets of cavities were shown: the smallest ones close to the free surface (grey bubbles in figure a) were shown as grey stars, whereas the bulk ones (blue bubbles in Figure 12 (c)) were represented by black stars except three of them, delayed, shown as unfilled stars in Figure 12 (c) and circled bubbles in Figure 12 (c).

A boundary layer with no detected cavities was observed following the sharp decrease of the gas content at the edge of the sample, which has previously been seen in some studies [21]. Indeed, at the first detected stages (150-200 seconds), curves corresponding to distances to the edge up to 300 $\mu$ m already exhibited a significant departure from saturation. The nucleation and growth of cavities with a maximum volume smaller than the resolution could have occurred within this boundary layer but was not detected from the  $\mu$ CT images.

The small edge cavities (grey series) appeared at about 150-200 seconds after decompression, a little bit deeper into the sample. Their maximum volume was reached at times between 350 and 550 seconds, whereas the deflation of most of the bulk cavities started from 600-700 seconds.

The main new observation provided by Figure 12 was that the maximum volume was observed for local partial pressures between 6 and 8 MPa (saturation) for the three types of cavities. A correlation with macroscopic desorption was thus evidenced. This partial pressure range was consistent also with the fact that some bulk cavities which did not deflate completely at the end of the tomography scan; the partial pressure calculated in the core of the sample after 3500 seconds was still above 6 MPa. This limiting partial pressure was more a range than a single critical value, probably due to other influence factors at the local scale, e.g. local heterogeneities of the rubber network and fluctuating maximal extensibility of the rubber at the cavity wall.

As mentioned in the earlier sections, the first detection of delayed cavities was at 350-500 seconds after decompression, exclusively in the bulk of the sample. At this time step, the curves corresponding to short distances to the edge have already dropped from saturation significantly, while curves referring to the bulk were still close to saturation. Hence, it could be said that the nucleation and growth of cavities was a local process.

As explained in the previous sections, edge cavities were seen to show a faster deflation and a shorter lifespan. This difference could be correlated with the different desorption rates following the maximum volume point (star mark) in edge and bulk curves. Dipping in the former curves was more important than observed in the latter ones. It could be concluded that the deflation rate of cavities could be correlated with the rapidity at which gradients evolved. Global desorption could be a driving force determining not only the maximum volume but also the full lifetime of isolated cavity.

To sum up, the nucleation and growth of cavities appeared as a local process while the deflation kinetics was highly influenced by macroscopic desorption. This was supported by looking at the global cavity field of the largest tested sample (Type-2) of EPDM 1.6 exposed to pressure conditions of  $P_{\text{sat}} = 12$  MPa and  $\dot{P} = 2.5$  MPa/min. Figure 13 (a) shows the initial stage where nucleation of cavities was seen to occur randomly throughout the sample. Figure 13 (b) shows the maximum volume stage of the cavity field and Figure 13 (c) shows the deflation stage where it could be evidenced that the deflation occurred as more of a global phenomenon giving the impression of a convex hull collapsing on itself. Again, it could be concluded that the deflation of the cavities was correlated with the decrease of the gas concentration in the sample as well as the rapidity at which this gradient evolved with time indicating that the global desorption was a major driving force determining the life of the cavity.

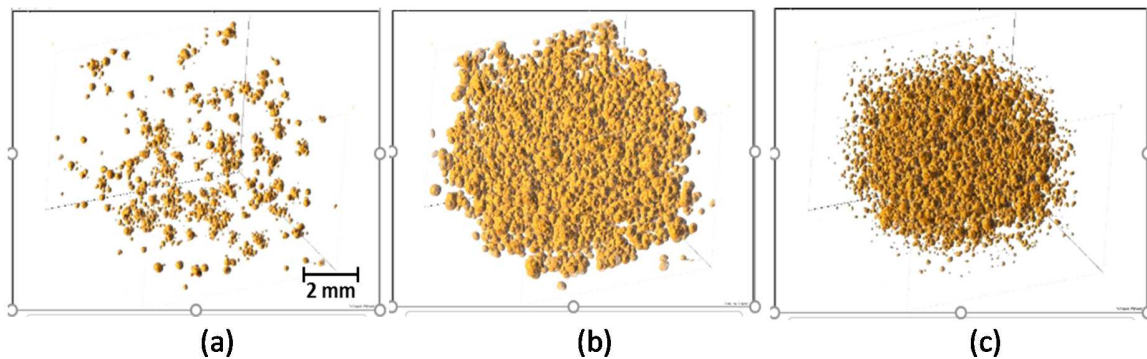


**Figure 13:** Global damage field of Type-2 sample of EPDM 1.6 exposed to  $P_{\text{sat}} = 12$  MPa and decompressed at 2.5 MPa/min at (a) early growth stage (b) maximum damage stage (c) deflation stage

#### 4. Conclusions

This work aimed at better understanding of decompression failure mechanisms in hydrogen-exposed rubbers under pressure, in a context of highly limited experimental access to the different physical fields. The objective was to discriminate more precisely various factors affecting growth kinetics of cavities at a local scale and to clarify interaction between cavities through comparative characterisation of isolated and close ones. This was done by conducting original in-situ X-ray tomography experiments in EPDM with different cross-link densities and different sample geometries, and under two different pressure conditions. The data from these experiments was analysed using image processing.

Since we were limited by the resolution of the tools, neither the very earliest stages of nucleation nor the very small distances between cavity edges were accessible for robust quantitative analysis. Within the present framework of material and experimental constraints, the following new conclusions were provided.

- By analysing the graphs for rate of inflation and the maximum volume attained by isolated cavities (in EPDM 1.6 as well as EPDM 0.5), two sets of cavities could be distinguished based on their growth kinetics. These cavities were termed as edge cavities and bulk cavities, a terminology that was based on the first order parameters governing their growth. The growth of edge cavities was strongly limited owing to the proximity to the free surface whereas the growth kinetics of bulk cavities were more determined by other factors such as time of nucleation or local boundary conditions.
- The interaction effects between close cavities (with borders at a minimum distance of 32 microns here due to the spatial resolution) was shown to be rather trivial. The kinetics of close cavities mimicked those of isolated ones, with other factors like distance to the free surface and time of nucleation being the first order parameters that drive the kinetics of inflation. The proximity to other cavities remains a second order parameter mainly affecting the topological isotropy of the cavities rather than growth kinetics.
- The classification of edge and bulk cavities was supported by the simulations carried out to see the temporal evolution of gradients of concentration along the sample geometry. There was good agreement between the experimental results and the diffusion simulation

that pointed to this edge effect (smaller maximum volume, faster deflation rate, shorter lifespan) being directly related to the macroscopic gas desorption.

- More generally, nucleation and growth appeared as local processes while deflation was more related to macroscopic desorption. This is of high interest for future definition of modeling strategies for sealing components.

## Acknowledgements

Authors would like to acknowledge the French Government programs “Investissements d’Avenir” LABEX INTERACTIFS (reference ANR-11-LABX-0017-01) for granting Mahak Fazal’s PhD, and EQUIPEX GAP (reference ANR-11-EQPX-0018) for supporting the development of the in-situ tomography experiment. As engineer in charge of tomography in the research group, Mr. David Mellier is gratefully acknowledged for his support to the X-ray tomography experiments.

## Data availability statement

The raw/processed data required to reproduce these findings cannot be shared at this time as the data also forms part of an ongoing study.

## References

- [1] R. L. Denecour and A. N. Gent, “Bubble formation in vulcanized rubbers,” *J. Polym. Sci. Part A-2 Polym. Phys.*, vol. 6, no. 11, pp. 1853–1861, Nov. 1968.
- [2] B. J. Briscoe, T. Savvas, and C. T. Kelly, “‘Explosive decompression failure’ of rubbers: a review of the origins of pneumatic stress induced rupture in elastomers,” *Rubber Chem. Technol.*, vol. 67, no. 3, pp. 384–416, 1994.
- [3] B. J. Briscoe and D. Liatsis, “Internal Crack Symmetry Phenomena during Gas-Induced Rupture of Elastomers,” *Rubber Chem. Technol.*, vol. 65, no. 2, pp. 350–373, May 1992.
- [4] B. Schritteser, G. Pinter, T. Schwarz, Z. Kadar, and T. Nagy, “Rapid Gas Decompression Performance of elastomers – A study of influencing testing parameters,” *Procedia Struct. Integr.*, vol. 2, pp. 1746–1754, 2016.
- [5] M. Melnichuk, F. Thiébaud, and D. Perreux, “Non-dimensional assessments to estimate decompression failure in polymers for hydrogen systems,” *Int. J. Hydrogen Energy*, vol. 45, no. 11, pp. 6738–6744, 2020.
- [6] Y.-T. Shieh, J.-H. Su, G. Manivannan, P. H. C. Lee, S. P. Sawan, and W. Dale Spall, “Interaction of supercritical carbon dioxide with polymers. I. Crystalline polymers,” *J. Appl. Polym. Sci.*, vol. 59, no. 4, pp. 695–705, Jan. 1996.
- [7] O. Lorge, B. J. Briscoe, and P. Dang, “Gas induced damage in poly (vinylidene fluoride) exposed to decompression,” *Polymer (Guildf.)*, vol. 40, no. 11, pp. 2981–2991, 1999.
- [8] P. Embury, “High-pressure gas testing of elastomer seals and a practical approach to designing for explosive decompression service,” *Seal. Technol.*, vol. 2004, no. 6, pp. 6–11, 2004.
- [9] S. Zakaria, “Why rubber explodes,” *Chemtech*, vol. 20, no. 8, pp. 492–495, 1990.

- [10] A. N. Gent, "Cavitation in rubber – a cautionary tale," *Rubber Chem. Technol.*, vol. 63, pp. G49–G53, 1990.
- [11] A. N. Gent and D. A. Tompkins, "Nucleation and growth of gas bubbles in elastomers," *J. Appl. Phys.*, 1969.
- [12] C. W. Stewart, "Nucleation and Growth of Bubbles in Elastomers," *J. Polym. Sci. Part A-2 Polym. Phys.*, vol. 8, pp. 937–955, 1970.
- [13] A. Stevenson and G. Morgan, "Fracture of elastomers by gas decompression," *Rubber Chem. Technol.*, vol. 68, pp. 197–211, 1995.
- [14] Z. Major, K. Lederer, T. Schwarz, and R. W. Lang, "Development of a test and failure analysis methodology for elastomeric seals exposed to rapid gas decompression in oilfield applications," *Eng. Struct. Integr. Res. Dev. Appl.*, vol. 12, pp. 754–757, Jan. 2007.
- [15] M. Najipour, L. Haroonabadi, and A. Dashti, "Assessment of failures of nitrile rubber vulcanizates in rapid gas decompression (RGD) testing: Effect of physico-mechanical properties," *Polym. Test.*, vol. 72, Nov. 2018.
- [16] D. Mori and K. Hirose, "Recent challenges of hydrogen storage technologies for fuel cell vehicles," *Int. J. Hydrogen Energy*, vol. 34, no. 10, pp. 4569–4574, May 2009.
- [17] N. Takeichi *et al.*, "'Hybrid hydrogen storage vessel', a novel high-pressure hydrogen storage vessel combined with hydrogen storage material," *Int. J. Hydrogen Energy*, vol. 28, no. 10, pp. 1121–1129, Oct. 2003.
- [18] J. Yamabe and S. Nishimura, "Influence of fillers on hydrogen penetration properties and blister fracture of rubber composites for O-ring exposed to high-pressure hydrogen gas," *Int. J. Hydrogen Energy*, vol. 34, no. 4, pp. 1977–1989, Feb. 2009.
- [19] J. Yamabe and S. Nishimura, "Crack Growth Behavior of Sealing Rubber under Static Strain in High-Pressure Hydrogen Gas," *J. Solid Mech. Mater. Eng.*, vol. 5, pp. 690–701, Jan. 2011.
- [20] S. Castagnet, J. C. Grandidier, M. Comyn, and G. Benoît, "Mechanical Testing of Polymers in Pressurized Hydrogen: Tension, Creep and Ductile Fracture," *Exp. Mech.*, vol. 52, no. 3, pp. 229–239, Mar. 2012.
- [21] J. Jaravel, S. Castagnet, J. C. Grandidier, and G. Benoît, "On key parameters influencing cavitation damage upon fast decompression in a hydrogen saturated elastomer," *Polym. Test.*, vol. 30, no. 8, pp. 811–818, Dec. 2011.
- [22] J. Jaravel, S. Castagnet, J. C. Grandidier, and M. Gueguen, "Experimental real-time tracking and diffusion/mechanics numerical simulation of cavitation in gas-saturated elastomers," *Int. J. Solids Struct.*, vol. 50, no. 9, pp. 1314–1324, Mar. 2013.
- [23] N. C. Menon, A. M. Kruizenga, K. J. Alvine, C. S. Marchi, A. Nissen, and K. Brooks, "Behaviour of polymers in high pressure environments as applicable to the hydrogen infrastructure," in *American Society of Mechanical Engineers, Pressure Vessels and Piping Division (Publication) PVP*, 2016, vol. 6B-2016.
- [24] A. Koga, K. Uchida, and J. Yamabe, "Evaluation on High-Pressure Hydrogen Decompression Failure of Rubber O-ring Using Design of Experiments," *Int. J. Automot. Eng.*, vol. 2, pp. 123–129, Jan. 2011.
- [25] O. Kane-Diallo, S. Castagnet, A. Nait-Ali, G. Benoit, and J. C. Grandidier, "Time-resolved statistics of cavity fields nucleated in a gas-exposed rubber under variable decompression conditions - Support to a relevant modeling framework," *Polym.*

- Test.*, vol. 51, pp. 122–130, 2016.
- [26] M. F. Butler, A. M. Donald, and A. J. Ryan, “Time resolved simultaneous small- and wide-angle X-ray scattering during polyethylene deformation—II. Cold drawing of linear polyethylene,” *Polymer (Guildf.)*, vol. 39, no. 1, pp. 39–52, 1998.
- [27] A. N. Gent and P. B. Lindley, “Internal rupture of bonded rubber cylinders in tension,” *Proc. R. Soc. London. Ser. A. Math. Phys. Sci.*, vol. 249, no. 1257, pp. 195–205, 1959.
- [28] J. M. Ball, “Discontinuous equilibrium solutions and cavitation in nonlinear elasticity,” *Philos. Trans. R. Soc. London. Ser. A, Math. Phys. Sci.*, vol. 306, no. 1496, pp. 557–611, 1982.
- [29] O. Lopez-Pamies, M. I. Idiart, and T. Nakamura, “Cavitation in elastomeric solids: I - A defect-growth theory,” *J. Mech. Phys. Solids*, vol. 59, no. 8, pp. 1464–1487, 2011.
- [30] X. Poulain, V. Lefèvre, O. Lopez-Pamies, and K. Ravi-Chandar, “Damage in elastomers: nucleation and growth of cavities, micro-cracks, and macro-cracks,” *Int. J. Fract.*, vol. 205, no. 1, pp. 1–21, 2017.
- [31] J. G. Murphy and S. Biwa, “Nonmonotonic cavity growth in finite, compressible elasticity,” *Int. J. Solids Struct.*, vol. 34, no. 29, pp. 3859–3872, 1997.
- [32] S. Xin-Chun and C. Chang-Jun, “Exact solution for cavitating bifurcation for compressible hyperelastic materials,” *Int. J. Eng. Sci.*, vol. 39, no. 10, pp. 1101–1117, 2001.
- [33] J. Dollhofer, A. Chiche, V. Muralidharan, C. Creton, and C. Y. Hui, “Surface energy effects for cavity growth and nucleation in an incompressible neo-Hookean material - Modeling and experiment,” *Int. J. Solids Struct.*, vol. 41, no. 22–23, pp. 6111–6127, 2004.
- [34] H. Hang-Sheng and R. Abeyaratne, “Cavitation in elastic and elastic-plastic solids,” *J. Mech. Phys. Solids*, vol. 40, no. 3, pp. 571–592, 1992.
- [35] B. J. Lee and M. E. Mear, “Studies of the growth and collapse of voids in viscous solids,” *J. Eng. Mater. Technol.*, vol. 116, no. 3, pp. 348–358, 1994.
- [36] J. Jaravel, S. Castagnet, J.-C. Grandidier, and M. Gueguen, “Experimental real-time tracking and diffusion/mechanics numerical simulation of cavitation in gas-saturated elastomers,” *Int. J. Solids Struct.*, vol. 50, no. 9, pp. 1314–1324, 2013.
- [37] E. Euchler, R. Bernhardt, K. Schneider, G. Heinrich, S. Wießner, and T. Tada, “In situ dilatometry and X-ray microtomography study on the formation and growth of cavities in unfilled styrene-butadiene-rubber vulcanizates subjected to constrained tensile deformation,” *Polymer (Guildf.)*, vol. 187, p. 122086, 2020.
- [38] S. Castagnet, D. Mellier, A. Nait-Ali, and G. Benoit, “In-situ X-ray computed tomography of decompression failure in a rubber exposed to high-pressure gas,” *Polym. Test.*, vol. 70, pp. 255–262, Sep. 2018.
- [39] J. Yamabe and S. Nishimura, “20 - Hydrogen-induced degradation of rubber seals,” in *Woodhead Publishing Series in Metals and Surface Engineering*, vol. 2, R. P. Gangloff and B. P. B. T.-G. H. E. of M. in E. T. Somerday, Eds. Woodhead Publishing, 2012, pp. 769–816.
- [40] H. Ono, A. Nait-Ali, O. Kane Diallo, G. Benoit, and S. Castagnet, “Influence of pressure cycling on damage evolution in an unfilled EPDM exposed to high-pressure

- hydrogen,” *Int. J. Fract.*, vol. 210, no. 1–2, pp. 137–152, Mar. 2018.
- [41] H. Ono, H. Fujiwara, and S. Nishimura, “Penetrated hydrogen content and volume inflation in unfilled NBR exposed to high-pressure hydrogen—What are the characteristics of unfilled-NBR dominating them?,” *Int. J. Hydrogen Energy*, vol. 43, no. 39, pp. 18392–18402, 2018.
- [42] J. Crank and P. Nicolson, “A practical method for numerical evaluation of solutions of partial differential equations of the heat-conduction type,” *Math. Proc. Cambridge Philos. Soc.*, vol. 43, no. 1, pp. 50–67, 1947.
- [43] S. Castagnet, J.-C. Grandidier, M. Comyn, and G. Benoît, “Mechanical Testing of Polymers in Pressurized Hydrogen: Tension, Creep and Ductile Fracture,” *Exp. Mech.*, vol. 52, no. 3, pp. 229–239, 2012.
- [44] A. N. Gent, “Cavitation in Rubber: A Cautionary Tale,” *Rubber Chem. Technol.*, 2011.
- [45] W. Henry, “Experiments on the Quantity of Gases Absorbed by Water, at Different Temperatures, and under Different Pressures,” *Philos. Trans. R. Soc. London*, vol. 93, pp. 29–276, May 1803.